

Observations of Small Large-Amplitude Magnetic Structures (SLAMS) at Mars by MAVEN

Kim Konstantin ¹, Shuvalov Sergey ¹

¹Space Research Institute of the Russian Academy of Sciences, Moscow, Russia

Key Points:

- The observed plasma structures are associated with Small Large-Amplitude Magnetic Structures
- The acceleration of O^+ and O_2^+ ions is the result of wave-particle interaction via Landau damping of ULF waves with H^+ ions

Corresponding author: Kim Konstantin, kimki@iki.rssi.ru

Abstract

According to the different orientations of the interplanetary magnetic field (IMF), the planetary shock can be either quasi-parallel or quasi-perpendicular. Under quasi-parallel conditions a significant number of solar wind suprathermal particles are reflected from the shock and drift along IMF, forming an extended and highly turbulent region called the foreshock where various nonlinear plasma phenomena are observed. In this research, we perform a case study of the structures in the foreshock region at Mars observed by Mars Atmosphere and Volatile Evolution (MAVEN). We use data from plasma analyzer STATIC and magnetometer MAG to analyze ion beams angular spectrum and magnetic field dynamics. We show that the observed structures are consistent with Short Large-Amplitude Magnetic Structures (SLAMS), commonly detected in foreshock regions of magnetized and unmagnetized bodies throughout the Solar system. Finally, we calculate the magnetic Mach number to analyze the characteristics of the observed foreshock structures. The analysis shows, that SLAMS are formed by the resonance between plasma waves propagating along the IMF and the backstreaming scattered solar wind H^+ and exospheric O^+ and O_2^+ ions, with the dominant impact of O_2^+ ions.

1 Introduction

The solar wind interaction with the Martian plasma environment has been actively investigated for the past few decades. One of the mostly discussed research areas is the solar wind interactions with planetary plasma environment. As the supersonic solar wind flow becomes subsonic at closer distances to Mars, a bow shock is formed at which solar wind is decelerated, deflected and thermalized. The observation of the Martian bow shock suggests the existence of the region upstream of the bow shock filled with ULF waves, diffusive ions and electrons. This region is known as foreshock region, which is forming under quasi-parallel shock conditions. In foreshock numerous plasma phenomena occur. The largest structures observed in the foreshock are foreshock cavities (Sibeck et al., 2002), foreshock bubbles (Turner et al., 2013) and hot flow anomalies (Schwartz et al., 1985; Thomsen et al., 1986; Paschmann et al., 1988).

The wave-particle interaction of ULF waves and ions under quasi-parallel shock conditions may lead to the formation of Short Large-Amplitude Magnetic Structures (SLAMS). The observations of SLAMS at terrestrial foreshock are described as long pulsations on a short time interval (Schwartz & Burgess, 1991; Schwartz et al., 1992; Wilson III et al., 2013). To date, SLAMS have been already observed at Venus (Omidi et al., 2017), Saturn (Bebesi et al., 2019) and Jupiter (Tsurutani et al., 1993), comets (Tsurutani et al., 2013). On Mars there are evident observations of SLAMS presence (Halekas et al., 2017; Collinson et al., 2018). However, the impact on the modulation of energetic neutral atoms flux by foreshock structures like SLAMS on Mars was described by (Fowler et al., 2019), but no analysis of SLAMS themselves was conducted. Also, there is an insight on the physical model of SLAMS formation at terrestrial foreshock as observed by Magnetospheric Multiscale (MMS) Mission (Chen et al., 2021).

This article provides the results of the SLAMS analysis during near-radial interplanetary magnetic field (IMF) conditions observed by Mars Atmosphere and Volatile Evolution (MAVEN) mission. We analyze plasma properties of foreshock ions upstream SLAMS formation region and solar wind ions both upstream and downstream SLAMS. We use minimum variance analysis technique to investigate wave nature of the observed process.

We analyze plasma properties of foreshock ions upstream SLAMS formation region and solar wind ions both upstream and downstream SLAMS. We use minimum variance analysis technique to investigate wave nature of the observed process.

2 Instrumentation

This research is based on the data obtained from MAVEN spacecraft, launched on 13 November 2013. MAVEN is inserted on an elliptical orbit around Mars with an orbital period of 4.5 hours. Its periapsis is at 150 km and apoapsis at 6200 km with 75° inclination. Data from magnetometer MAG and Suprathermal And Thermal Ion Composition (STATIC) instrument from the Particle and Fields package is used in this study.

STATIC is a top-hat ion energy-mass analyzer (McFadden et al., 2015). The instrument measures the ion energy distribution in a wide energy range from 0.1 eV to 30 keV and can resolve H^+ , O^+ and O_2^+ ions, covering ionospheric, magnetospheric and tail plasma. Its field of view (FOV) is 360°x90° which is decreasing at high energies, with angular resolution 22.5°x22.5°. The energy resolution of the instrument is $dE/E \sim 15\%$ and mass resolution is $M/dM \geq 4$. During the data analysis routine, the contamination of H^+ mass channel is considered. The data sampling rate can be switched from 4 to 16 sec, and was 4 sec during the analyzed time interval.

The MAG measures 3 components of local magnetic field in the solar wind, magnetosheath and crustal magnetic field with 32 Hz time cadance (Connerney et al., 2015). Its dynamic range is 60000 nT with a resolution is 0.05 nT.

3 Observation

The event was detected in a time interval within 02.00 – 02.30 UT 23 October 2019. The observed orbit of MAVEN lies through the dayside of Mars, crossing the subsolar region from the northern to the southern hemisphere of Mars. The altitude varies from 500 to 2000 km. The observational period is divided into two regions: oscillation region from 02.00 to 02.25 UT and solar wind region from 02.25 to 02.30 UT. The solar wind conditions are characterized by narrow energy spectra of H^+ ions with the maximum energy flux approximately at 1 keV and a weakly disturbed magnetic field. The (IMF) vector averaged over the solar wind region has components [4.1020 -1.1556 0.6414] nT in Mars Solar Orbital (MSO) frame, in which x-axis is pointed to the Sun, y-axis is directed against the orbital motion of the planet, and z-axis completes the system to the right-handed basis. Considering orbital characteristics and IMF conditions, the observed oscillation region is consistent with the foreshock region.

The data from STATIC and MAG is demonstrated in form of time series in Figure 1. Starting from 02.00 UT quasi-periodic pulsations of the magnetic field, accompanied by deceleration of H^+ ions, are observed. The pulsations of the magnetic field have a period of 66 ± 36.6 sec and a time width of approximately 12 sec. The magnetic field in the structures increases by factor of 4 to 8 compared to the total value of IMF.

No significant correlation between ion density variations and magnetic field pulsations are observed, despite the time interval from 02.12 to 02.15 UT, where peaks of magnetic field pulsations coincide with minimums of light-to-heavy ion density ratio.

The Figure 2 demonstrates an example of a typical angular distribution function during SLAMS crossing from 02.22 to 02.24 UT. Hammer projection is used to show the measured part of velocity space by STATIC instrument. Each bin corresponds to one angular cell with sizes $25^\circ \times 25^\circ$ and the color of the bin shows the differential energy flux. We also consider a feature of STATIC FOV by which it is narrowing as the measured energy increases. The direction of the local magnetic field is shown as a red cross. The MSO basis vectors of frame $\{X_{MSO}, Y_{MSO}, Z_{MSO}\}$ in STATIC frame are shown by red, green and black dots and circles respectively, highlighting the positive and negative directions. Empty angular distribution functions are neglected.

The detailed analysis of the H^+ ion angular distribution function (ADF) in Figure 2 shows the observation of two ion beams: the solar wind H^+ ions beam and foreshock H^+ ions. The solar wind is seen as a narrow ion beam with high differential energy flux in the sunward (X_{MSO+}) direction. At the same time foreshock ions are characterized by wide angular distribution detected near the direction of IMF. The typical ADF of H^+ ions is seen from 02.25.11 to 02.25.19 UT which corresponds to the upstream region of SLAMS in Figure 1. At 02.25.07 UT the process of deceleration and heating of the solar wind is seen. The energy of ions on average decreases by 4-5 times and the angular coverage of FOV by the solar wind ions is significantly higher, compared to the upstream region. From 02.24.45 to 02.25.07 UT the ions beam population of low energy scattered H^+ ions is observed propagating in the direction of IMF. At the same time O^+ and O_2^+ ADF shows the appearance of narrow ion beams in the sunward and pick-up ions in anti-sunward directions.

The presence of the scattered/deflected ion beam is the consequence of the solar wind interaction with the bow shock-like sharp front of SLAMS. As result, the interaction of the deflected ion beams with Alfvén waves is described by Landau damping. Comparing phase velocity of Alfvén wave v_A and peak velocity v of the solar wind H^+ ions EDA, we see that $v > v_A$. Thus energetic ions transfer their energy to the Alfvén wave modulating the amplitude of SLAMS.

4 Analysis

In further chapters, the results of the case study will be performed and discussed. In a time interval from 02.22 to 02.26 UT, only several events have clear observations of the magnetic field oscillations and plasma properties.

4.1 Minimum Variance Analysis of magnetic field oscillations (MVAB)

We apply MVAB to calculate the wave vector k of magnetic field B oscillations. We also assume that the observed oscillations are more temporal rather than spatial due to the specific process of SLAMS formation. To estimate the orientation of the wave vector k the condition of $(k, B) = 0$ should be considered. According to MVAB, solving the eigenvalue and eigenvector problem for matrix $M = \langle B_i B_j \rangle - \langle B_i \rangle \langle B_j \rangle$, where $i, j = \{x, y, z\}$, results as three vectors B_{max} , B_{int} , B_{min} of maximum, intermediate and minimum variance of magnetic field respectively. In B_{max} , B_{int} , B_{min} frame wave activity in a given time interval looks like rotation in one of the planes which is clearly seen in Figure 3. If the rotation is in the B_{max} and B_{int} plane, then it gives a rough estimation of the line, which contains k and $B_{min} \parallel k$. The direction of the wave vector is chosen based on the physical conditions of the processes that occurred in foreshock.

The major results of MVAB are listed in Table 1. It is seen that the observed waves propagate along with the IMF into the Sun direction. The polarization of waves is both left-handed and right-handed. Though data can't provide accurate information about H^+ temperature due to different problems, we assume plasma is cold. In cold magnetoactive plasma, several types of wave modes exist. As the observed waves have $k \parallel B$, they are possibly Alfvén or magnetosonic waves. The relation of B_{\parallel}/B_{\perp} shows that the waves have major oscillations perpendicular to magnetic field direction, thus we assume that observed waves have Alfvén nature.

4.2 Wavelet analysis

To go deeper with the wave analysis, we apply continuous wavelet transform (CWT) on the magnetic field with the Morlet wavelet. In Figure 4a the CWT is demonstrated for the whole period of time. The colorbar is indicating the square module of the amplitude. In the time interval from 02.12 to 02.16 UT, strong oscillations near O^+ and O_2^+

ions cyclotron frequency are observed. A normalized general wavelet spectrum (GWS) with overlaying mean value and standard deviation of cyclotron frequencies of H^+ , O^+ and O_2^+ ions is shown in Figure 4b. It is seen that O_2^+ cyclotron frequency corresponds to the global maximum of GWS. At the same time, H^+ and O^+ cyclotron frequencies are located in the vicinity of GWS local maximums. This pattern proves the hypothesis of ultra-low frequency Alfvén waves observation, which originates from the solar wind interaction with Martian quasi-parallel bow shock. We also observe an intensive interaction between Alfvén waves and O_2^+ ions in foreshock region.

4.3 SLAMS shock characteristics

One of the most interesting features of SLAMS is their shock characteristics. To investigate the shock parameters of SLAMS, shock normal and the angle between the IMF and shock normal for SLAMS and bow shock are calculated. The formula for calculation of the normal vector to shock surface of rotational discontinuity requires the values of the magnetic field upstream and downstream of the shock. The upstream magnetic field was averaged in the vicinity of SLAMS, and the downstream magnetic field was averaged in the core of SLAMS. The results of the calculation are listed in Table 2. The average duration of the magnetic field amplification is 12.6 ± 3.72 sec, the angle between the bow shock and IMF on average is $\Theta_{Bn} = 14.9 \pm 0.9$, which is consistent with quasi-parallel bow shock. The SLAMS shock parameters are varying drastically compared to bow shock, however, the average angle between the normal vector of SLAMS and IMF is less than 45° . This means SLAMS may inherit the configuration of the bow shock.

The dynamics of solar wind during the interaction with planetary bow shock can be described by magnetic Mach number $M_A = v_{sw}/v_A$, with v_{sw} – solar wind velocity, $v_A = B/\sqrt{4\pi np}$ – Alfvén velocity of H^+ ions. The Alfvén velocity is important physical parameter in space plasma, which closely related to the wave activity. If $M_A > 1$, then the solar wind velocity has supersonic values; if $M_A < 1$ – the solar wind velocity is subsonic. High Mach numbers ($M_A > 1$) are typical for the solar wind in the upstream region. As the solar wind interacts with the bow shock, the solar wind decelerates, the total magnetic field is increasing by 2-3 times according to the Rankine-Hugoniot conditions. All this factors cause the decrease of magnetic Mach number to subsonic values. Previously, we showed that SLAMS can have shock nature.

In Figure 5 the scatterplot of Mach number and density of H^+ ions is shown. The colorbar indicates the ratio of the measured magnetic field to the total value of IMF. Two populations of H^+ ions are seen on the scatterplot with different density and Mach number. The labeled with red color distribution of density and Mach number indicates the solar wind H^+ ions, and labeled with blue indicates the shocked H^+ ions. Pretty logical to assume less dense and faster ion population as an upstream H^+ ions of the solar wind.

4.4 Wave-particle interaction of ULF waves and foreshock ions

Considering MAVEN altitude during the analyzed time interval, the observed backstreaming O^+ and O_2^+ ions are originated from the Martian exosphere. The energies of these ions far exceed the thermal energies of exospheric ions. One of the possible mechanisms for the growth of the ion energies might be Landau damping. As shown in Section 4.1, the observed ULF waves are propagating along the IMF and interact with exospheric ions. The Figure 6 represents the comparison of calculated average velocities of backstreaming H^+ , O^+ and O_2^+ ions with Alfvén velocity, which is considered as phase velocity of the observed waves.

The peak velocities of O^+ and O_2^+ ions correspond to 17.5 and 24.3 km/s, respectively, which is lower than mean Alfvén velocity (around 34.9 km/s). At the same time,

H^+ maximum velocity is around 126.9 km/s, which is higher compared to Alfvén velocity. In terms of wave-particle interaction this observation can be interpreted as a complex multicomponent plasma interaction. The backstreaming H^+ ions transfer their kinetic energy to ULF waves, amplifying them via Landau damping mechanism. Then, amplified ULF waves transfer energy to O^+ and O_2^+ , accelerating them to suprathermal velocities in the sunward direction.

5 Conclusion and discussion

In conclusion, this article performs the case study of foreshock structures, commonly known as Short Large-Amplitude Magnetic Structures, in the time interval 02.20 to 02.30 UT of 23 October 2019. On the time scale of roughly tens of seconds, the magnetic field amplifies by a factor of 4-5 times compared to IMF. The MVAB applied on the time interval of SLAMS observation shows the presence of ULF Alfvén and magnetosonic waves, which are originated from the interaction of the solar wind ions and backstreaming ions. It was found by the wavelet analysis that O_2^+ ions cyclotron frequency is the dominant observed frequency in the oscillations of the magnetic field. The possible explanation is the high inertia of O_2^+ ions, compared to O^+ and H^+ ions. The shock parameters of SLAMS are inherited from the planetary bowshock, having the same quasi-parallel structure.

The observed process of O^+ and O_2^+ ions acceleration from thermal to suprathermal velocities is not analyzed in this article. Though, the proposed mechanism of Landau damping during the wave-particle interaction seems logical, more analysis should be done.

Acknowledgments

The authors of the article are grateful to the Russian Scientific Foundation (RSF). The research is supported by RSF grant 21-42-04404. We also would like to thank MAVEN team for providing data, Andrey Malykhin and Elena Grigorenko for productive discussions.

References

- Bebesi, Z., Erdos, G., & Szego, K. (2019). Observations of short large amplitude magnetic structures at the kronian bow shock. *Icarus*, 333, 306-317. doi: <https://doi.org/10.1016/j.icarus.2019.06.023>
- Chen, L.-J., Wang, S., Ng, J., Bessho, N., Tang, J.-M., Fung, S. F., ... Burch, J. (2021). Solitary magnetic structures at quasi-parallel collisionless shocks: Formation. *Geophysical Research Letters*, 48(1), e2020GL090800. doi: <https://doi.org/10.1029/2020GL090800>
- Collinson, G., Wilson III, L. B., Omid, N., Sibeck, D., Espley, J., Fowler, C. M., ... Jakosky, B. (2018). Solar wind induced waves in the skies of mars: Ionospheric compression, energization, and escape resulting from the impact of ultralow frequency magnetosonic waves generated upstream of the martian bow shock. *Journal of Geophysical Research: Space Physics*, 123(9), 7241-7256. doi: <https://doi.org/10.1029/2018JA025414>
- Connerney, J. E. P., Espley, J., Lawton, P., Murphy, S., Odom, J., Oliverson, R., & Sheppard, D. (2015, December). The MAVEN Magnetic Field Investigation. , 195(1-4), 257-291. doi: 10.1007/s11214-015-0169-4
- Fowler, C. M., Halekas, J., Schwartz, S., Goodrich, K. A., Gruesbeck, J. R., & Benna, M. (2019). The modulation of solar wind hydrogen deposition in the martian atmosphere by foreshock phenomena. *Journal of Geophysical Research: Space Physics*, 124(8), 7086-7097. doi: <https://doi.org/10.1029/2019JA026938>

- Halekas, J. S., Ruhunusiri, S., Harada, Y., Collinson, G., Mitchell, D. L., Mazelle, C., ... Jakosky, B. M. (2017). Structure, dynamics, and seasonal variability of the mars-solar wind interaction: Maven solar wind ion analyzer in-flight performance and science results. *Journal of Geophysical Research: Space Physics*, 122(1), 547-578. doi: <https://doi.org/10.1002/2016JA023167>
- McFadden, J. P., Kortmann, O., Curtis, D., Dalton, G., Johnson, G., Abiad, R., ... Jakosky, B. (2015, December). MAVEN SupraThermal and Thermal Ion Composition (STATIC) Instrument. , 195(1-4), 199-256. doi: 10.1007/s11214-015-0175-6
- Omidi, N., Collinson, G., & Sibeck, D. (2017). Structure and properties of the foreshock at venus. *Journal of Geophysical Research: Space Physics*, 122(10), 10,275-10,286. doi: <https://doi.org/10.1002/2017JA024180>
- Paschmann, G., Haerendel, G., Sckopke, N., Möbius, E., Lühr, H., & Carlson, C. W. (1988). Three-dimensional plasma structures with anomalous flow directions near the earth's bow shock. *Journal of Geophysical Research: Space Physics*, 93(A10), 11279-11294. doi: <https://doi.org/10.1029/JA093iA10p11279>
- Schwartz, S. J., & Burgess, D. (1991, March). Quasi-parallel shocks: A patchwork of three-dimensional structures. , 18(3), 373-376. doi: 10.1029/91GL00138
- Schwartz, S. J., Burgess, D., Wilkinson, W. P., Kessel, R. L., Dunlop, M., & Luehr, H. (1992, April). Observations of Short Large-Amplitude Magnetic Structures at a Quasi-Parallel Shock. , 97(A4), 4209-4227. doi: 10.1029/91JA02581
- Schwartz, S. J., Chaloner, C. P., Christiansen, P. J., Coates, A. J., Hall, D. S., Johnstone, A. D., ... Woolliscroft, L. J. C. (1985, November). An active current sheet in the solar wind. , 318(6043), 269-271. doi: 10.1038/318269a0
- Sibeck, D. G., Phan, T.-D., Lin, R., Lepping, R. P., & Szabo, A. (2002). Wind observations of foreshock cavities: A case study. *Journal of Geophysical Research: Space Physics*, 107(A10), SMP 4-1-SMP 4-10. doi: <https://doi.org/10.1029/2001JA007539>
- Thomsen, M. F., Gosling, J. T., Fuselier, S. A., Bame, S. J., & Russell, C. T. (1986). Hot, diamagnetic cavities upstream from the earth's bow shock. *Journal of Geophysical Research: Space Physics*, 91(A3), 2961-2973. doi: <https://doi.org/10.1029/JA091iA03p02961>
- Tsurutani, B. T., Arballo, J. K., Smith, E. J., Southwood, D., & Balogh, A. (1993). Large-amplitude magnetic pulses downstream of the jovian bow shock: Ulysses observations. *Planetary and Space Science*, 41(11), 851-856. (Special Issue: Ulysses Flyby of Jupiter) doi: [https://doi.org/10.1016/0032-0633\(93\)90092-G](https://doi.org/10.1016/0032-0633(93)90092-G)
- Tsurutani, B. T., Echer, E., Richter, I., Koenders, C., & Glassmeier, K.-H. (2013). Slams at comet 19p/borrelly: Dsl observations. *Planetary and Space Science*, 75, 17-27. doi: <https://doi.org/10.1016/j.pss.2012.11.002>
- Turner, D. L., Omidi, N., Sibeck, D. G., & Angelopoulos, V. (2013). First observations of foreshock bubbles upstream of earth's bow shock: Characteristics and comparisons to hfas. *Journal of Geophysical Research: Space Physics*, 118(4), 1552-1570. doi: <https://doi.org/10.1002/jgra.50198>
- Wilson III, L. B., Koval, A., Sibeck, D. G., Szabo, A., Cattell, C. A., Kasper, J. C., ... Wilber, M. (2013). Shocklets, slams, and field-aligned ion beams in the terrestrial foreshock. *Journal of Geophysical Research: Space Physics*, 118(3), 957-966. doi: <https://doi.org/10.1029/2012JA018186>

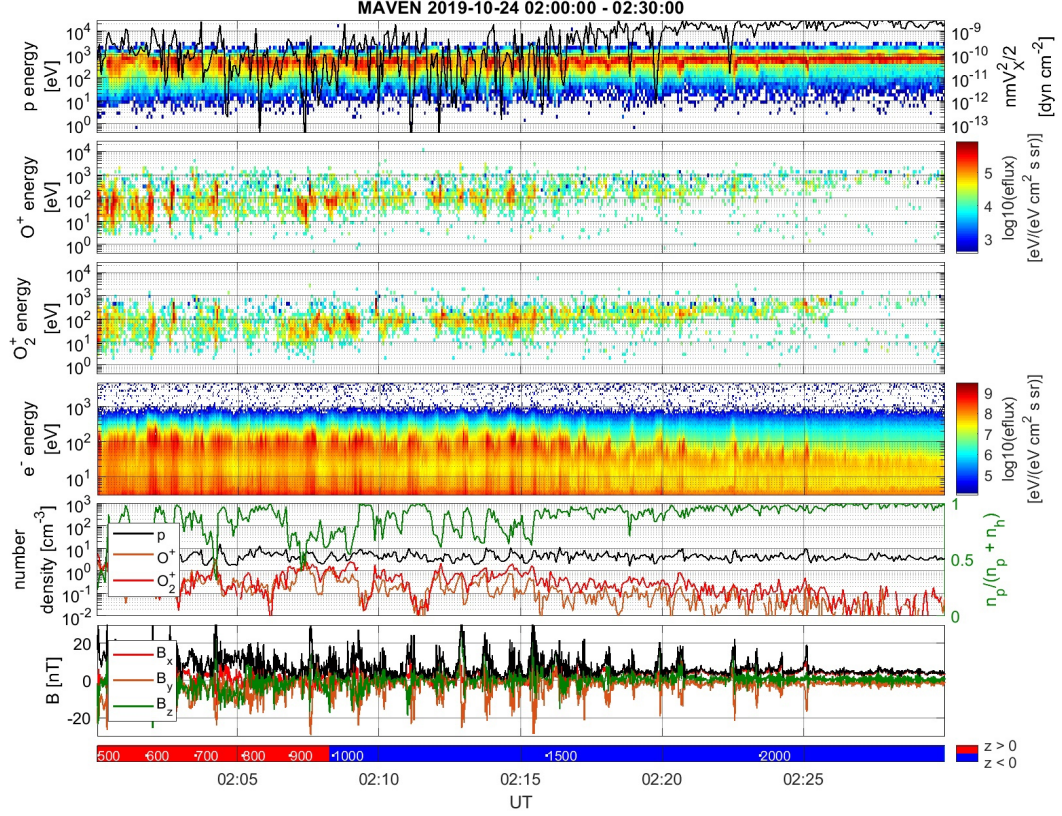


Figure 1. Observation of SLAMS at 24 October 2019 in a time interval from 02:00:00 to 02:30:00 (from up to the bottom): energy-time spectrograms of H^+ , O^+ and O_2^+ ions and electrons; number density of H^+ , O^+ and O_2^+ ions, and light to heavy ions ratio overlaid; vector of magnetic field

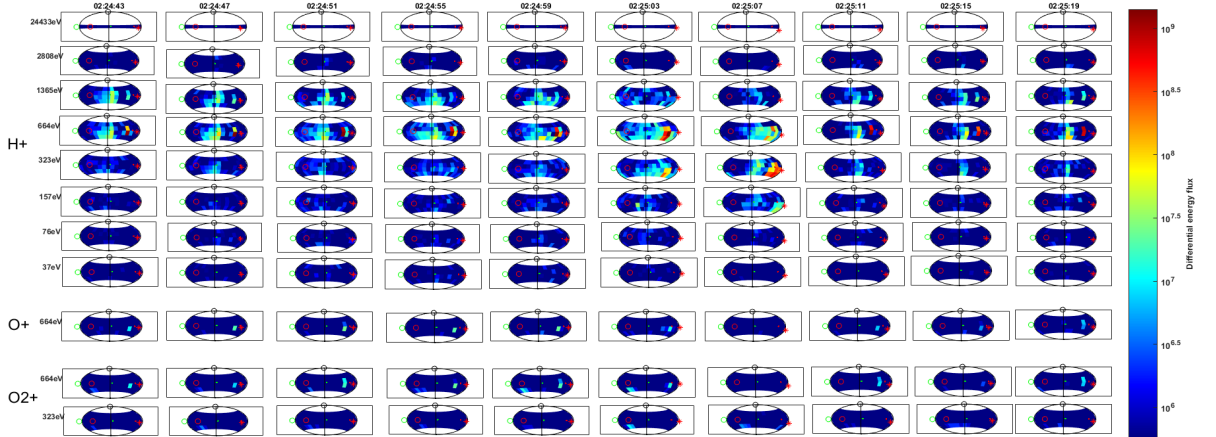


Figure 2. An example of ion angular distribution function of H^+ , O^+ and O_2^+ ions. Red cross corresponds to the IMF direction in STATIC frame. Red, green and blue dot and circles corresponds to XMSO, YMSO and ZMSO in STATIC frame, where dots and circles indicate positive and negative direction of each axis, respectively

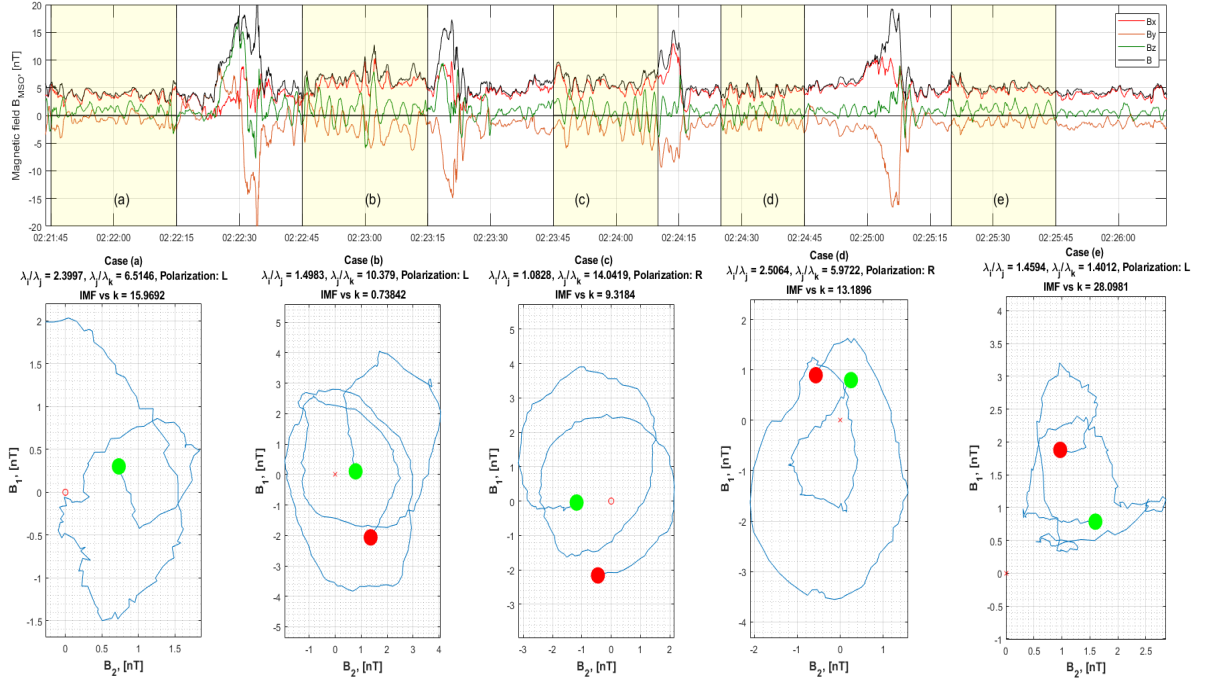


Figure 3. The results of MVAB for the time interval from 02.22 to 02.26 UT. Green and red dots correspond to the beginning and end of the time interval. With dot and cross the direction of vector k is demonstrated

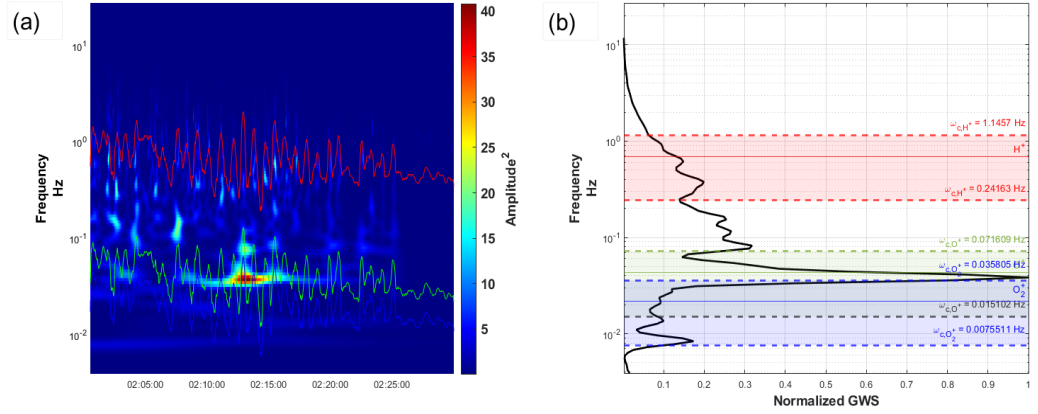


Figure 4. (a) Wavelet spectrum of the magnetic field and (b) General Wavelet Spectrum (GWS). Colored areas indicate confidence interval for cyclotron frequencies of H^+ , O^+ and O_2^+ ions

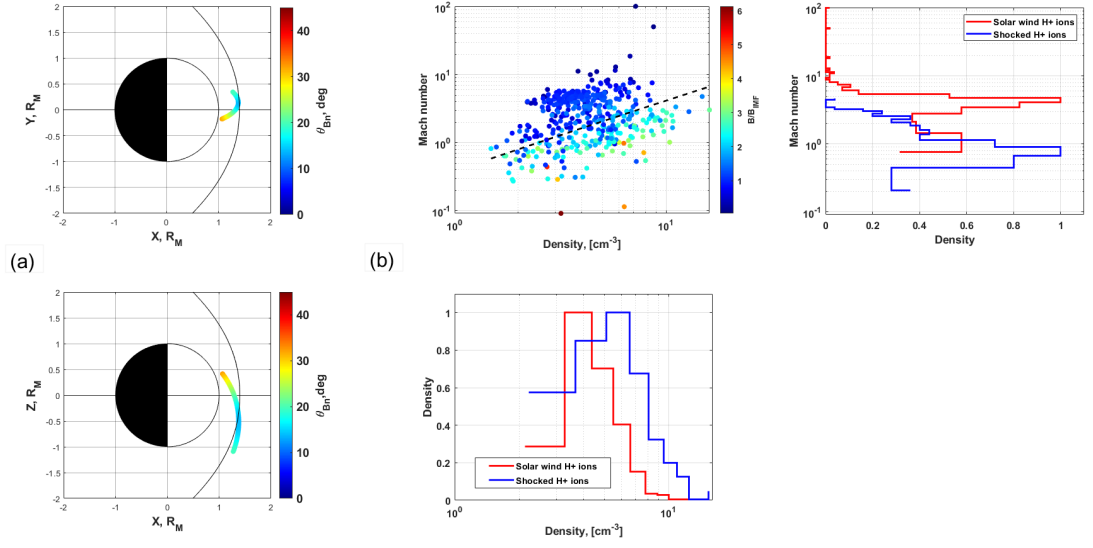


Figure 5. (a) MAVEN orbit projections (colorbar shows the angle between the magnetic field and normal to the bow shock Θ_{Bn}), (b) scatterplot of H^+ ions density and magnetic Mach number

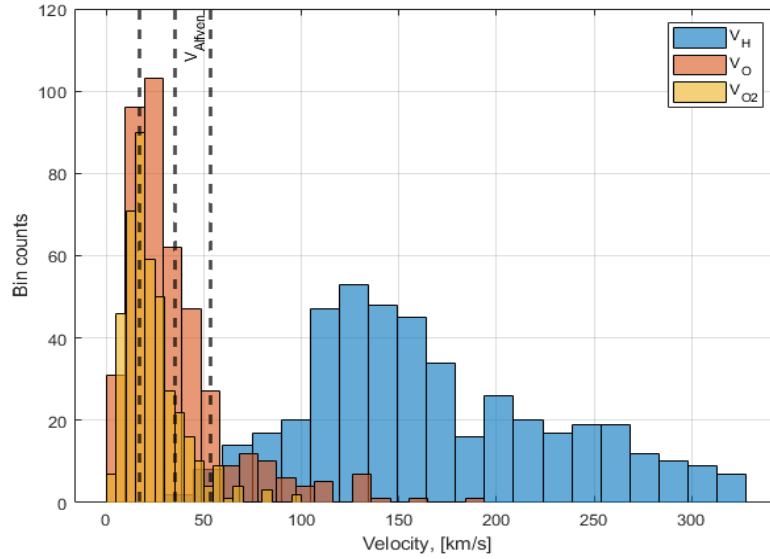


Figure 6. Comparison of the backstreaming H^+ , O^+ and O_2^+ ions velocities with the Alfvén velocity

Table 1. The calculated characteristics of the observed waves

Event	Time, UT	B_{max}/B_{int}	B_{int}/B_{min}	k	IMF vs k , deg	Polarization	B_{\parallel}/B_{\perp}
a	02.22.00 - 02.22.04	2.4	6.5	[0.98 0.01 0.18]	15.9	L	3.6
b	02.22.48 - 02.22.58	1.5	10.4	[0.96 -0.26 0.14]	0.7	L	2.2
c	02.24.00 - 02.24.05	1.1	14.1	[0.93 -0.22 0.30]	9.3	R	2.2
d	02.24.35 - 02.24.40	2.5	5.9	[0.91 -0.19 0.36]	13.2	R	2.3
e	02.25.30 - 02.25.35	1.4	1.4	[0.75 -0.29 0.59]	28	L	4.3

Table 2. Model shock parameters compared with SLAMS shock parameters in the time period of 02:00:00 - 02:30:00 24 October 2019.

Observation time, UT	Duration, s	n_{BS}	Θ_{Bn} , deg	n_{SLAMS}	Θ'_{Bn} , deg
02:24:47 - 02:25:47	10	[0.92 -0.11 0.38]	16.31	[0.88 0.47 0.11]	43.32
02:23:55 - 02:24:39	5	[0.93 -0.09 0.36]	15.79	[0.63 0.75 0.23]	64.57
02:23:11 - 02:23:39	8	[0.93 -0.09 0.35]	15.28	[0.93 0.26 -0.27]	39.41
02:22:15 - 02:22:47	10	[0.94 -0.09 0.33]	14.86	[0.99 0.09 -0.08]	24.64
02:20:19 - 02:21:03	14	[0.95 -0.07 0.29]	14.16	[0.87 0.48 0.14]	43.90
02:19:39 - 02:20:19	14	[0.96 -0.06 0.28]	13.96	[0.97 -0.14 0.19]	7.82
02:18:39 - 02:19:27	12	[0.96 -0.05 0.26]	13.84	[0.93 0.35 0.15]	35.84
02:17:47 - 02:18:35	12	[0.97 -0.05 0.24]	13.83	[0.99 0.13 0.04]	23.99
02:13:27 - 02:14:19	22	[0.94 0 0.13]	15.55	[0.94 -0.02 0.3]	17.76
02:12:35 - 02:13:27	19	[0.99 0.01 0.11]	16.27	[0.75 -0.59 -0.28]	33.18
Mean value	12.60 ± 3.72	-	14.99 ± 0.85	-	33.43 ± 11.96